*Mineralogical Magazine, April 2016, Vol. 80(2), pp. 249–267*

OPEN ACCESS

# T-induced displacive phase transition of end-member Pb-lawsonite

MARTIN ENDE[1,*], BERND WUNDER[2], MONIKA KOCH-MÜLLER[2], THOMAS PIPPINGER[1], GERNOT BUTH[3], GERALD GIESTER[1], CHRISTIAN L. LENGAUER[1] AND EUGEN LIBOWITZKY[1]

[1] Department of Mineralogy and Crystallography, University of Vienna, 1090 Vienna, Austria
[2] Helmholtz-Zentrum Potsdam, GFZ German Research Centre for Geosciences, 14473 Potsdam, Germany
[3] ANKA, Karlsruhe Institute of Technology (KIT), 76131 Karlsruhe, Germany

[*Received 17 October 2014; Accepted 21 June 2015; Associate Editor: Mark Welch*]

**ABSTRACT**

Pb-lawsonite, $PbAl_2[(OH)_2|Si_2O_7]\cdot H_2O$, space group *Pbnm*, was synthesized as crystals up to 15 μm × 5 μm × 5 μm in size by a piston cylinder technique at a pressure of ~4 GPa and a temperature of 873 ± 10 K. Temperature-dependent powder and single-crystal X-ray diffraction (XRD) analyses partly using synchrotron radiation as well as Raman spectroscopic investigations reveal a phase transition around 445 K resulting in the *Cmcm* high-temperature structure. The transformation temperature is considerably higher than that of lawsonite around 273 K, which is characterized predominantly by proton order/disorder. The transition is confirmed using principal component analysis and subsequent hierarchical cluster analysis on both the powder XRD patterns and the Raman spectra. Furthermore, a non-uniform change is observed around 355 K, which is not as pronounced as the 445 K transition and apparently comes from enhanced hydrogen bonding, which stops the atom shifts in Pb-lawsonite. These are the same bonds that mainly characterize the phase transition in lawsonite around 273 K. In contrast, the structural transition of Pb-lawsonite at 445 K seems to originate from the interaction of the $SiO_4$ tetrahedra and $AlO_6$ octahedra framework with the $Pb^{2+}$ cation. The structural environment of $Pb^{2+}$ can be described by a 12-fold coordination above 445 K, which changes towards irregular ten-fold coordination below this temperature. An assignment of the O–H stretching Raman bands confirms moderately strong H bonds in Pb-lawsonite, whereas both strong and weak H bonds exist in lawsonite. Therefore, a further phase transition of Pb-lawsonite, similar to that of lawsonite around 273 K, is not expected.

**KEYWORDS:** lawsonite, Pb-lawsonite, structural phase transition, principal component analysis, PCA.

## Introduction

LAWSONITE-TYPE compounds $A^{+2}B_2^{+3}[(OH)_2|C_2O_7]\cdot H_2O$ ($A$ = Ca, Sr, Ba, Pb; $B$ = Al, Mn, Fe; $C$ = Si, Ge) are high density (3.09 g cm$^{-3}$ for lawsonite, 4.53 g cm$^{-3}$ for Pb-lawsonite) hydrous disilicates (except for Ge), which are stable over a broad *P–T* field (Schmidt and Poli, 1994; Daniel *et al.*, 1999; Pawley and Allan, 2001). Mostly, chains of $AlO_6$ octahedra plus $Si_2O_7$ dimers build up a mixed polyhedral framework, in which large $A$ cations, $OH^-$ groups and $H_2O$ molecules fill the structure voids (Fig. 1). Because of the high $H_2O$ content and its extensive structural stability at high pressure, lawsonite ($CaAl_2[(OH)_2|Si_2O_7]\cdot H_2O$) *sensu stricto* is considered a potential carrier for $H_2O$ into the subduction zones of the Earth (Daniel *et al.*, 1999; Brovarone and Beyssac, 2014). In the last two decades, more and more lawsonite-type compounds with different compositions have been found in nature, i.e. hennomartinite (Sr-$Mn^{3+}$-silicate; Armbruster *et al.*, 1993), noélbensonite (Ba-$Mn^{3+}$-silicate; Kawachi and Coombs, 1996), itoigawaite (Sr-Al-silicate; Miyajima *et al.*, 1999),

* E-mail: martin.ende@univie.ac.at
DOI: 10.1180/minmag.2016.080.015

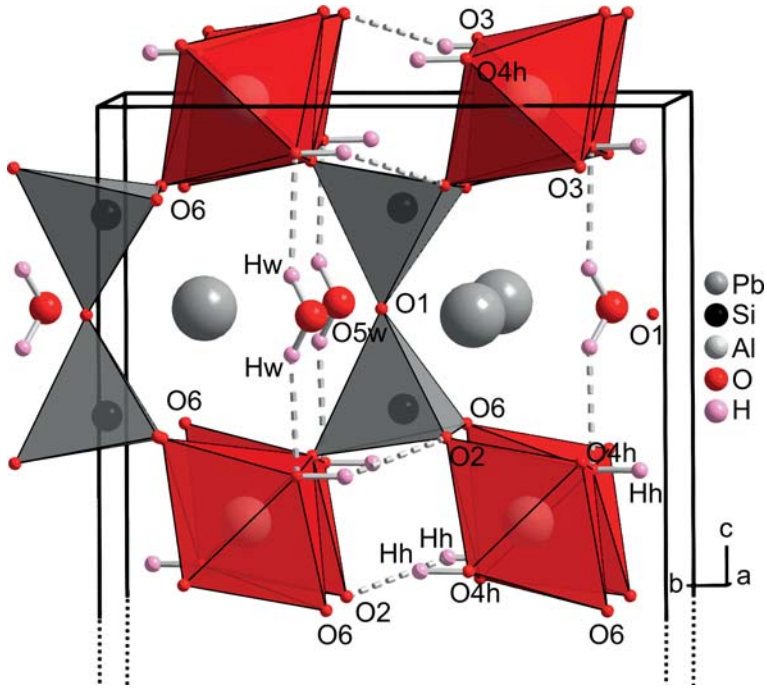


FIG. 1. Part of the unit cell of Pb-lawsonite, space group *Pbnm*, at room temperature. Broken grey lines indicate H bonds with H···O distances of 1.95 to 2.06 Å.

Cr-lawsonite (Ca-(Al,Cr)-silicate, Mevel and Kienast, 1980; Sherlock and Okay, 1999), and more recently bartelkeite (Pb-Fe-germanate; Origlieri *et al.*, 2012). Libowitzky and Armbruster (1995) found that lawsonite shows phase transitions at 273 and 150 K. These transitions mainly involve changes in the positions of the hydrogen atoms and their immediate neighbours together with modifications in the hydrogen-bond scheme. Libowitzky and Rossman (1996) indicated dynamically disordered hydroxyl groups and $H_2O$ molecules for the room temperature *Cmcm* structure of lawsonite. By referring to the smooth changes of stretching and bending frequencies in infrared (IR) spectra across the phase boundaries they suggested a phase transition of a dynamic order-disorder type.

After successful synthesis and characterization of Sr-lawsonite (Liebscher *et al.*, 2010), Pb-lawsonite was first synthesized and structurally characterized using powder samples by Dörsam *et al.* (2011). The aim of the present paper is to present single-crystal structure data and to trace the temperature-dependent structural transformations of Pb-lawsonite using Raman spectroscopic and powder XRD measurements, including principal component analysis (PCA) and subsequent cluster analysis on both data sets. In addition, the structures of the high-temperature phases were investigated by single-crystal and powder XRD.

## Synthesis and experiments

For synthesis of Pb-lawsonite Dörsam *et al.* (2011) used a mixture of α-quartz, γ-$Al_2O_3$, PbO and NaCl in water. In our study the starting material used was an amorphous glass with stoichiometric Pb-lawsonite cation composition ($PbAl_2Si_2O_{x(7–8)}$) and microporous properties (micro- to nano-particles sintered in a spongy structure), aimed at obtaining faster growth rates compared to Dörsam *et al.* (2011), who produced only fine-grained material in their experiments.

The stoichiometric glass was synthesized using the Pechini or citrate gel method (Pechini, 1967; Raab, 2010) with slightly more than 0.03 M tetraethyl orthosilicate ($C_8H_{20}O_4Si$) as the silicon source. Furthermore, 0.03 M of citric acid and 0.06 M of ethylene-glycol were used to produce around 0.015 M of the precursor phase with 0.03 M $Al(NO_3)_3 \cdot 9H_2O$, $Pb(NO_3)_2$ and 0.015 M tetraethyl-orthosilicate at 438 K for 12 h. The resulting precursor phase was milled and calcined at 923 K for 12 h. The glass

was sealed together with excess water in Au capsules 10 mm × 2 mm × 2 mm in size, compressed at 4 GPa, heated within 30 min to ~873 K and kept constant under these conditions for ~120 h. A standard piston cylinder apparatus with NaCl assembly and steel furnace was used. Pressure could be controlled within ±50 MPa and temperature was recorded with a Ni-Cr-Ni thermocouple with an accuracy of ±10 K, based on calibrations with reference substances. The thermocouple was placed close to the centre of the capsule.

## Experimental

### *Raman spectroscopy*

Powder samples with a grain size of <1 μm were used. Spectra were acquired with a Renishaw RM1000 micro-Raman spectrometer with a 20 mW 632.8 nm HeNe laser, a 1200 $mm^{-1}$ grating, and a thermoelectrically cooled CCD detector. All measurements were accomplished with a resolution of ~2.5 $cm^{-1}$. Spectra were measured in 180° back-scattering geometry on a Linkam (THMS 600) cooling-heating stage using a 20x/0.40 long distance objective. The precision of the measured temperature of the stage is ~0.1 K, but the temperature of the sample may differ over a range of 5 K according to its size, its position on the stage and the influence of the supporting glass plate. The laser power at the sample was reduced to ~3 mW to avoid heating the sample, and the glass plate was mounted on the silver block of the cooling-heating stage. The system was calibrated to the Rayleigh line and the Raman line of a silicon wafer with respect to the stress-free value of 520 $cm^{-1}$. Based on low laser power and very small sample amounts the measurements were started at room temperature with 2 × 20 min and were increased every 5 K to ~2 × 30 min at 573 K.

For evaluation of Raman band positions and peak widths (full width at half maximum, FWHM) a pseudo-Voigt function with a free mixing factor of Gauss and Lorentz components was used to fit the bands. In addition a multivariate statistical technique, principal component analysis (PCA; Pearson, 1901) plus subsequent hierarchical cluster analysis were performed. PCA for Raman spectroscopy, for example, was successfully applied by Sato-Berru *et al.* (2007) and Mejía-Uriarte *et al.* (2012) for the characterization of $BaTiO_3$ phase transitions.

### *Single-crystal diffraction and powder X-ray diffraction*

The room temperature single-crystal structure analysis was performed using a Bruker Kappa Apex II diffractometer with a CCD detector and an Incoatec Microfocus Source IμS (30 mW, multilayer mirror, Mo$K\alpha$, 0.71 Å). The high-temperature single-crystal XRD experiment at 370 K was performed at the SCD beam line at ANKA, the synchrotron radiation facility at KIT in Karlsruhe, Germany. The chosen wavelength was 0.8 Å in combination with a 62 mm × 62 mm CCD Bruker AXS SMART APEX detector of 60 μm resolution. During the high-temperature measurement, an Oxford Cryosystems low-temperature device was used as a regulated hot air blower (±0.1 K; range 80–400 K). Data treatment (integration, scaling) was performed with the *APEX2* suite of programs (Bruker, 2014). Reflection patterns were in accordance with space group *Pbnm* for both the room temperature and 370 K structures. Experimental details of data collection and structure determination are summarized in Table 1. The programmes *Jana2006* (Petříček *et al.*, 2006) and *SHELX* (Sheldrick, 2008) were used for the single-crystal structure analyses. Refinements were based on $F^2$. All hydrogen atoms were found by difference-Fourier syntheses for the room temperature (RT) data set. They were not restrained with HFIX commands, as the refinement process revealed plausible electron density for the hydrogen positions with reliable, though shortened, oxygen–hydrogen distances. For the 370 K measurement the data quality did not allow us to find hydrogen positions or to refine the anisotropic displacement parameters for all the atoms. Isotropic factors were used for refinement instead. The displacement ellipsoids for the RT measurement are plausible.

Powder diffraction data were acquired using a Bruker D8 goniometer with a Paar XRK900 non-ambient device, a copper X-ray tube (40 kV, 40 mA) and Lynx-Eye position-sensitive detector. The measurements were from RT to 498 K in 5 K steps with 1 s per point and from 11–80°2θ using 0.01°2θ step widths. At 488 K an extended measurement with 2.5 s per step was performed for structure determination. The powder X-ray pattern at 488 K was refined with the Rietveld section of the program *GSAS* (Larson and Von Dreele, 1994; Rietveld, 1967) with the graphical user interface *EXPGUI* (Toby, 2001). For this purpose, a structure dataset with coordinates from a single-crystal refinement was modified and subsequently refined using the

TABLE 1. Crystal and experimental data of $PbAl_2[(OH)_2|Si_2O_7]\cdot H_2O$.

| Parameter | 298 K | 370 K | 488 K |
|---|---|---|---|
| *a* (Å) | 5.851(1) | 5.859(1) | 5.875(1) |
| *b* (Å) | 9.028(2) | 9.048(1) | 9.017(1) |
| *c* (Å) | 13.295(3) | 13.354(2) | 13.367(2) |
| *V* (Å$^3$) | 702.3(2) | 707.9(2) | 708.1(2) |
| Space group | *Pbnm* (no. 62) | *Pbnm* (no. 62) | *Cmcm* (no. 63) |
| $D_{calc}$ (g/cm$^3$)* | 4.553 | 4.517 | 4.516 |
| μ (mm$^{-1}$)* | 24.54 | 29.32 | 51.61 |
| *Z* | 4 | 4 | 4 |
| Crystal size (μm) | 15 × 15 × 6 | 8 × 5 × 5 | powder |
| Diffractometer | Bruker APEX II | SCD ANKA/KIT | Bruker D8 |
| Radiation | 0.71073 Å (Mo*K*α) | 0.8 Å | 1.5418 (Cu$K\alpha_{1,2}$) |
| $\theta_{min}$–$\theta_{max}$ (°) | 3.06–40.10 | 3.43–31.31 | 5.50–40.00 |
| No. of observed reflect. [$I > 3\sigma(I)$] | 12,689 | 2638 | 132 |
| No. of unique reflect.[$I > 3\sigma(I)$] | 1435 | 673 | 132 |
| No. of param. used in refinement | 80 | 37 | 20[b] |
| $R_{int}$ | 0.071 | 0.152 | – |
| $R_1$ (%) | 3.3[a] | 6.0[a] | 7.3[c] |
| $R_w$ ($R_2$) (%) | 5.2[a] | 13.0[a] | 9.8[c] |
| Goof | 1.10[a] | 1.92[a] | 1.39[c] |

*calculated for complete formula (including $H_2O$ and hydroxyl group).
[a]$R_1$, $R_2$ and Goof from *Jana2006* (Petříček *et al*., 2006) using $F^2$ weighting; [b]plus background terms; [c]$R_p$, $R_{wp}$ and Goof from *GSAS* (Larson and Von Dreele, 1994; Rietveld, 1967).

powder data. Restraints for $SiO_4$ tetrahedra, using Si–O and O–O bond distances from the 370 K single-crystal refinement with a variation of ±0.03 Å, were applied in order to obtain stable refinement. Selected crystal data and measurement details for the three different crystal structure refinements are summarized in Table 1.

## Results

### *Crystal growth*

The Pb-lawsonite crystals obtained by the piston cylinder experiments were transparent, clear, idiomorphic, mostly cube-shaped, but less commonly prismatic. However, the larger crystals show a pronounced prismatic shape with a maximum edge length of 20 μm and an average size of 15 μm × 5 μm × 5 μm (Fig. 2). There were no visible intergrowths. The crystallinity was proven to be sufficient with Raman spectroscopy as well as powder and single-crystal XRD. The purity of the synthesis batch was determined by powder XRD to be ~98 wt.%. Traces of coesite and an unidentified hydrated Pb carbonate were observed as additional phases. The size of the grains of the Pb-lawsonite matrix was <3 μm.

### *Raman spectroscopy*

Powder Raman spectra of Pb-lawsonite at different temperatures are shown in Figs 3 and 4. While Fig. 4 shows the region between 40 and 1140 cm$^{-1}$ with lattice vibrations, silicate and $AlO_6$ stretching vibrations, Fig. 3 presents the range from 2300 to 4000 cm$^{-1}$ where the stretching vibrations of the $H_2O$ molecule and the hydroxyl groups occur. In Fig. 4 it is obvious that an isolated group of bands between 780 and 1100 cm$^{-1}$ (intense at ~950 cm$^{-1}$) is clearly separated from a fairly uniform group of bands ranging from 42 to 480 cm$^{-1}$ and two bands at 553 and 667 cm$^{-1}$. Each of the $SiO_4$ tetrahedra in Pb-lawsonite is connected via O1 into $Si_2O_7$ dimers and are fixed with the six terminal O atoms to the relatively rigid chains of $AlO_6$ octahedra. Thus, the vibrational behaviour is different from isolated $SiO_4$ tetrahedra. Referring to Le Cléac'h and Gillet (1990), stretching vibrations of the $Si_2O_7$ dimers generally occur at wavenumbers above ~700 cm$^{-1}$ (Lazarev, 1972; Farmer, 1974; Kieffer, 1979, 1980; Hofmeister *et al.*, 1987) and can be divided into the stretching vibrations of $SiO_3$ terminal units (~800–1000 cm$^{-1}$) and the symmetric (~600–700 cm$^{-1}$) and

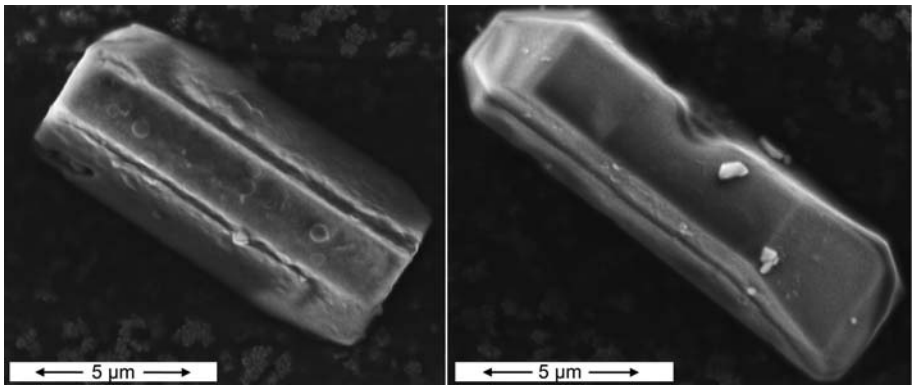


FIG. 2. Scanning electron microscopy – secondary electron images of two larger Pb-lawsonite crystals synthesized from $PbAl_2SiO_{x(7-8)}$ glass and excess water in a piston cylinder experiment at 600°C and 4 GPa.

antisymmetric (~1000–1200 $cm^{-1}$) stretching vibration of the Si–O–Si bridge (Lazarev, 1972; Gabelica-Robert and Tarte, 1979). Following Le Cléac'h and Gillet (1990), in lawsonite these vibrations start with $\nu_s$-Si–O–Si at 694 $cm^{-1}$ accompanied by a group of $SiO_3$ stretching vibrations with a maximum at 935 $cm^{-1}$ and end with $\nu_{as}$-Si–O–Si at 1047 $cm^{-1}$. In Pb-lawsonite the band pattern appears very similar to that of lawsonite at RT. One stronger band is observed at 667 $cm^{-1}$ ($\nu_s$-Si–O–Si) followed by a group with a maximum at 943 $cm^{-1}$ ($SiO_3$ stretching vibrations). The terminal band is at 1077 $cm^{-1}$ ($\nu_{as}$-Si–O–Si). Table 2 shows the band assignments of Pb-lawsonite, proposed by analogy with those of lawsonite (Le Cléac'h and Gillet, 1990). The stretching vibrations of the $H_2O$ molecule and the hydroxyl groups between 3150 and 3350 $cm^{-1}$ (RT) show a large temperature-induced shift. In particular, the band at 3329 $cm^{-1}$ (RT) exhibits a positive shift of >150 $cm^{-1}$ between 83 K and 573 K (Fig. 3). A weak band at 858 $cm^{-1}$ (RT) also shows a significant shift from 877 $cm^{-1}$ at 83 K to 799 $cm^{-1}$ at 573 K. The temperature-dependent band shifts reveal the same non-uniform changes for the band at 3329 $cm^{-1}$ (RT) as for the band at 858 $cm^{-1}$ (RT) (Fig. 5).

Further detailed investigations were made with the band around 858 $cm^{-1}$, starting at room temperature and going up to ~650 K with 5 K steps (Fig. 5). This band is relatively broad and comparable to a band in lawsonite at 809 $cm^{-1}$. Most probably it is not related to $SiO_3$ stretching vibrations (Libowitzky and Rossman, 1996), but

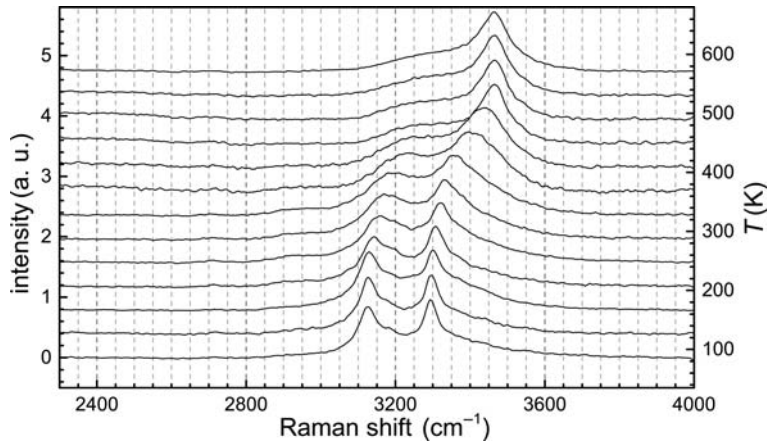


FIG. 3. Temperature-dependent Raman spectra of Pb-lawsonite from 83 to 573 K showing stretching vibrations of the hydroxyl groups and the $H_2O$ molecule. Spectra are vertically offset and smoothed only for presentation.

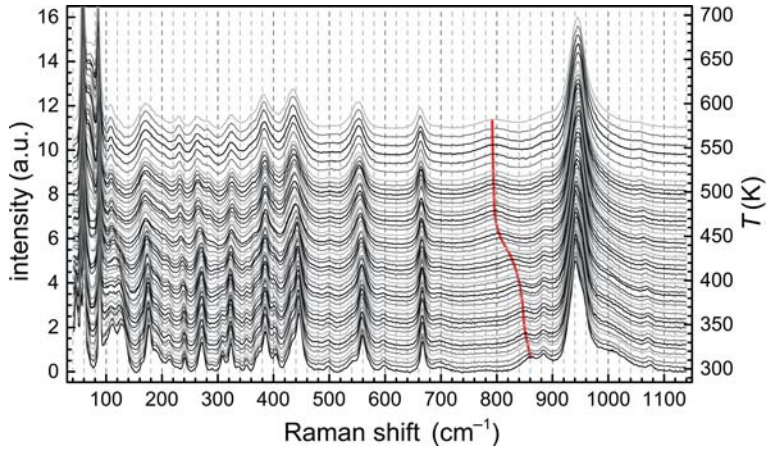


FIG. 4. Temperature-dependent Raman spectra of Pb-lawsonite from 298 to 573 K showing the vibrations of the $Si_2O_7$ groups and $AlO_6$ octahedra as well as lattice vibrations. Spectra are vertically offset. The bold line at ≈790–860 cm$^{-1}$ indicates the maximum of the γ-OH vibrational band.

rather arises from out-of-plane bending of a hydroxyl group, i.e. a so-called γ-OH vibration (Novak, 1974). Two clear non-uniform changes in the band shift are obvious around 355 and 445 K (Fig. 5). A principal component analysis was applied using the full spectra, including band positions and intensities, to confirm the significance of the band shifts. Subsequent hierarchical clustering, which joins similar observations and successively connects the next similar observations to these, was calculated with squared Euclidean distances. For the PCA a preceding scree test/plot (Cattel, 1966) was carried out to check the optimum usable factors, which represent the principal part of the variance. Instead of a correlation matrix, a covariance matrix was used. To prevent interaction with the Rayleigh line filter only the region from 75 to 1200 cm$^{-1}$ was taken into account for the analyses. The scree plot limited the meaningful selection of principal components to two or three. The first two principal components include 94.6% of the total variance of the original data and the subsequent Euclidean hierarchical cluster analysis shows plausible results, splitting the non-ambient data points into four meaningful groups (Fig. 6). These are separated by the temperatures of 353/358, 443/448 and 498/503 K. Both, the first and the second transition points are in good agreement with the band fitting method described above. A three times longer measuring time possibly causes the outlier at 298 K. The points in group 5 above 503 K may be split off due to the onset of dehydration. Raman spectroscopic measurements were also carried out from RT to 83 K. These data reveal no indication of any further non-uniform change or discontinuity.

TABLE 2. Raman band assignment for Pb-lawsonite and lawsonite (Le Cléac'h and Gillet, 1990) at room temperature. Band positions are reported in wavenumbers (Raman shift).

| Band position Pb-lawsonite | Band assignment | Band position lawsonite |
|---|---|---|
| 446 | δ/γ-Si–O–Si | 455[a] |
| 561 | δ-$SiO_3$ | 562[a] |
| 667 | $\nu_s$-Si–O–Si | 694 |
| 858 | γ-OH | 809[b] |
| 885–1012, 943 max. | ν-$SiO_3$ | 912–963, 935 max. |
| 1077 | $\nu_{as}$-Si–O–Si | 1047 |
| 1349 | δ-OH | – |
| 1489 | δ-$H_2O$ | 1578 |
| *c*. 3150–3350 | ν-$H_2O$/OH | *c*. 2960–3580[c] |

[a]Not assigned; [b]assumed as $AlO_6$ stretching vibration; [c]from IR study (Libowitzky and Rossman, 1996).

### *Single-crystal X-ray diffraction*

The crystal structure of Pb-lawsonite at room temperature, space group *Pbnm*, first derived from powder X-ray data by Dörsam *et al.* (2011), was confirmed (Tables 1 and 3). Estimates for the

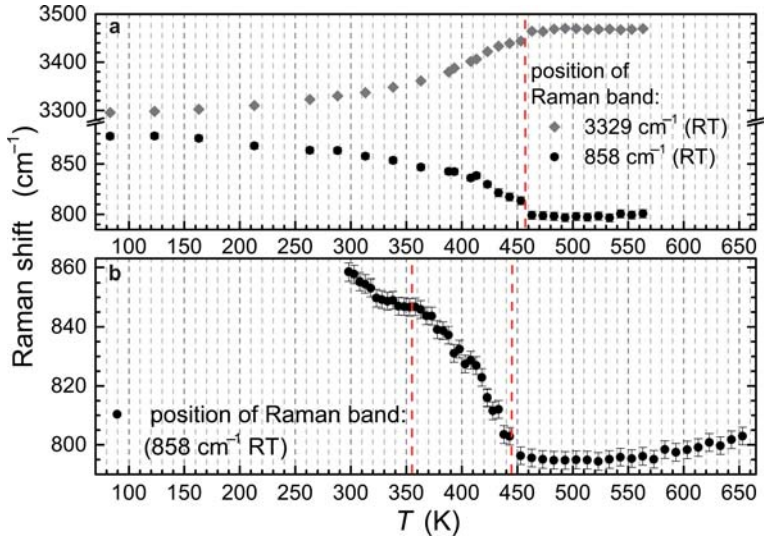


FIG. 5. Band shift analysis of two Raman bands. The band at 858 cm$^{-1}$ (RT) is assigned to an out-of-plane bending vibration of the hydroxyl group and the band at 3329 cm$^{-1}$ to a stretching vibration of the OH group. The lower plot shows two, clear, non-uniform changes, one around 355 K and the other around 445 K. The temperature behaviour of (*a*) and (*b*) is slightly different, possibly caused by the use of a single crystal (*a*) and Pb-lawsonite powder (*b*) for analysis.

hydrogen positions and anisotropic displacement parameters are presented in Tables 3 and 4. With a size of ~10 μm the crystal was very small and the $R_{int}$ value of 7.1% was relatively high. Nevertheless, a good fit was obtained (Table 1). The $R_{int}$ value of the 370 K synchrotron data was 13.0%. However, the crystal volume was 6–7 times smaller than the former (*c.f.* Table 1). The fits were calculated using *Jana2006* (Petříček *et al.*, 2006) and the integrated $F^2$ weighting. Refined atomic positions and displacement parameters for the single-crystal refinement are summarized in Table 5. Because of the small crystallite size of the 370 K sample only isotropic displacement parameters were refined, but these had to be manually fixed to 0.001 for Si and Al to gain a

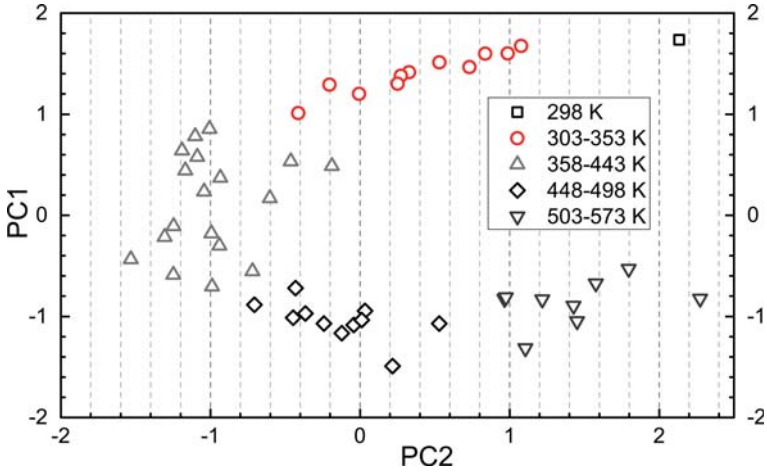


FIG. 6. Results of the principal component analysis with subsequent Euclidean hierarchical cluster analysis of the Raman spectra of Pb-lawsonite at different temperatures.

TABLE 3. Refined fractional atomic coordinates and equivalent anisotropic displacement parameters of orthorhombic Pb-lawsonite at room temperature (space group setting *Pbnm*).

| Atom | Wyck. | *x* | *y* | *z* | $100 \cdot U_{eq}$* (Å$^2$) |
|---|---|---|---|---|---|
| Pb | 4c | 0.02342(30) | 0.16182(20) | 0.25 | 0.95(6) |
| Si | 8d | 0.51116(16) | 0.01394(12) | 0.37034(80) | 0.44(2) |
| Al | 8d | 0.23638(18) | 0.75543(13) | 0.00238(90) | 0.43(2) |
| O1 | 4c | 0.53360(60) | 0.97730(40) | 0.25 | 0.77(7) |
| O2 | 8d | 0.74220(50) | 0.10030(30) | 0.40110(20) | 0.65(5) |
| O3 | 8d | 0.49280(40) | 0.85190(30) | 0.42680(20) | 0.58(5) |
| O4h | 8d | 0.02130(40) | 0.15210(30) | 0.55690(20) | 0.64(5) |
| O5w | 4c | 0.06840(90) | 0.87930(60) | 0.25 | 1.65(9) |
| O6 | 8d | 0.28720(40) | 0.11420(30) | 0.39170(20) | 0.68(5) |
| Hw | 8d | 0.012(9) | 0.842(8) | 0.203(7) | 5.00** |
| Hh | 8d | 0.040(8) | 0.068(6) | 0.556(4) | 0.80** |

Hydrogen and oxygen atoms of the $H_2O$ and hydroxyl groups are characterized with a 'w', i.e. Hw, O5w and an 'h', i.e. O4h, Hh.
*$U_{eq} = (U^{11}U^{22}U^{33})^{1/3}$; **$U_{iso}$.

stable fit. For Pb, anisotropic displacement parameters were refined and converged to $U^{11} = 0.0055(4)$, $U^{22} = 0.0028(5)$, $U^{33} = 0.0091(4)$ and $U^{13} = 0.0023(3)$ Å$^2$, which are all reasonable, though smaller than at RT. All tested specimens at 298 and 370 K exhibit more than one diffracting domain in the single-crystal XRD pattern, as evidenced by extra diffraction peaks. However, non-merohedral twinning could not be confirmed. No apparent differences between the crystal structures of Pb-lawsonite at 298 and 370 K were found; a possible explanation for the non-uniform change of the Raman and X-ray data around 355 K is given below.

### *Powder X-ray diffraction*

The space group suggested by using the PANalytical X'pert software *HighScore* at 488 K was *Cmcm* and thus corresponds to one of the minimal non-isomorphic supergroups of space group *Pbnm (Pnma*). Moreover, it is identical to that of the room-temperature structure of lawsonite. To compare the unit-cell dimensions and the atom positions directly with the *Cmcm* setting of Pb-lawsonite at 488 K the non-standard space group setting *Pbnm* was used instead of *Pnma* for the lower-temperature phases. Thus, Pb-lawsonite in space group *Pbnm* is obtained by a 'klassengleiche'

TABLE 4. Anisotropic displacement parameters (x100) of orthorhombic Pb-lawsonite at room temperature (space group setting *Pbnm*).

| | $U^{11}$ (Å$^2$) | $U^{22}$ (Å$^2$) | $U^{33}$ (Å$^2$) | $U^{12}$ (Å$^2$) | $U^{13}$ (Å$^2$) | $U^{23}$ (Å$^2$) |
|---|---|---|---|---|---|---|
| Pb | 0.976(9) | 0.933(9) | 0.946(10) | 0.132(8) | 0 | 0 |
| Si | 0.51(4) | 0.47(4) | 0.34(4) | 0.03(3) | –0.03(3) | 0. 03(3) |
| Al | 0.43(5) | 0.44(4) | 0.41(5) | 0.04(4) | –0.07(4) | 0.00(4) |
| O1 | 1.07(15) | 0.74(16) | 0.49(18) | 0.32(14) | 0 | 0 |
| O2 | 0.80(10) | 0.45(11) | 0.78(13) | 0.01(9) | 0.10(10) | –0.30(10) |
| O3 | 0.75(11) | 0.38(10) | 0.60(12) | –0.10(8) | –0.07(8) | 0.11(9) |
| O4h | 0.93(11) | 0.26(10) | 0.73(13) | 0.01(10) | 0.02(9) | 0.19(9) |
| O5w | 2.40(20) | 1.80(20) | 0.80(20) | –0.57(18) | 0 | 0 |
| O6 | 0.61(11) | 0.61(11) | 0.76(14) | 0.11(9) | –0.13(9) | –0.08(10) |

TABLE 5. Refined fractional atomic coordinates and isotropic displacement parameters of orthorhombic Pb-lawsonite at 370 K (space group setting *Pbnm*).

| Atom | Wyckoff | *x* | *y* | *z* | $100 \cdot U_{iso}$ (Å$^2$) |
|---|---|---|---|---|---|
| Pb | 4c | 0.02130(11) | 0.16171(9) | 0.25 | 0.58(2)[a] |
| Si | 8d | 0.5106(5) | 0.0135(4) | 0.3701(3) | 0.1[b] |
| Al | 8d | 0.2381(6) | 0.7549(5) | 0.0021(3) | 0.1[b] |
| O1 | 4c | 0.5291(18) | 0.9766(14) | 0.25 | 0.3(3) |
| O2 | 8d | 0.7417(14) | 0.1008(11) | 0.3998(7) | 0.7(2) |
| O3 | 8d | 0.4932(11) | 0.8523(10) | 0.4269(7) | 0.11(18) |
| O4h | 8d | 0.0198(12) | 0.1509(10) | 0.5573(8) | 0.33(18) |
| O5w | 4c | 0.063(2) | 0.8797(18) | 0.25 | 1.0(4) |
| O6 | 8d | 0.2869(14) | 0.1133(11) | 0.3914(7) | 0.5(2) |

[a]$U_{eq} = (U^{11}U^{22}U^{33})^{1/3}$, [b]fixed value.

symmetry reduction of index two (k2) from the *Cmcm* high-temperature space group (Hahn, 2005; Wondraschek and Müller, 2010). Regarding only the type of symmetry relationship, this is a similar k2 reduction as for lawsonite (*Cmcm* – *Pmcn*) at 273 K (Libowitzky and Armbruster, 1995) and hennomartinite (*Cmcm* – *Pmcn*) at 423 K (Libowitzky and Armbruster, 1996). However, it has different directions of symmetry reduction and a different role of H atoms (see below). Analyses of the powder patterns measured in 5 K steps from RT up to 498 K confirm the phase transition of Pb-lawsonite from *Pbnm* to *Cmcm*. The (101), (103), (121) and (212) diffraction peaks, forbidden by the extinction rule for *C* centring, can only be observed at lower temperatures in the primitive space group, are progressively weaker above 350 K and are absent above 450 K (arrows in Fig. 7). In contrast, the (110) peak, which has nearly the same intensity at RT as the (101) peak and fulfils the reflection condition of space group *Cmcm*, is constantly present, even above 450 K (Fig. 7).

Again, for a first overview, a PCA with subsequent hierarchical cluster analysis was made from the powder XRD data by using a covariance matrix. A prefixed scree plot (Cattel, 1966) limited the meaningful selection of principal components to two or three. As the first two components represent more than 88.6% of the total variance of the original data, and as the cluster analysis showed distinct results, the choice of three principal components was disregarded. The clustering of

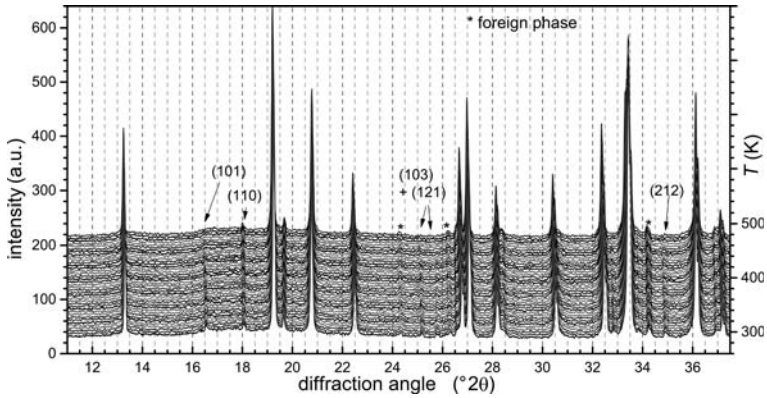


FIG. 7. Powder XRD patterns of Pb-lawsonite ($T$ = 298 to 498 K) showing the phase transition from space group *Pbnm* to *Cmcm* around 450 K. The XRD patterns were smoothed and vertically offset to enhance the visibility of the small diffraction peaks. Arrows indicate a number of weak, critical reflections and their indices.

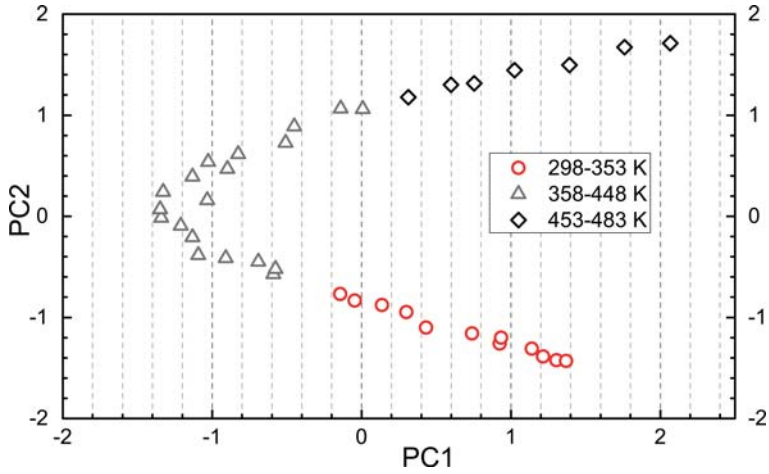


FIG. 8. Results from a principal component analysis with subsequent hierarchical cluster analysis of the temperature-dependent Pb-lawsonite powder X-ray pattern data.

each two points, which was seen in a previous analysis and which was due to the mechanical shift, carried out for compensation of the thermal expansion of the sample holder, was reduced by a mathematical correction of the displacement shifts causing a higher noise in the present PCA analysis. The PCA analysis (Fig. 8) now shows a smooth change in the diffraction data between the determined transition points and a distinct jump from 353 to 358 K. The hierarchical cluster analysis reveals three groups, which are separated at 353–358 K and 448–453 K and thus indicates nearly the same transition temperatures as obtained with Raman spectroscopy.

At first glance, the lattice parameters, which were obtained by LeBail refinements (LeBail, 1988) of the diffraction patterns using *TOPAS* (Coelho, 2007), did not show this behaviour. Nevertheless, knowledge of the possible transition points enabled a good fit of an exponential decay function ($A \cdot \exp^{(x/t)} + y_0$) to the data points between them (Fig. 9). The deviation, Δ, from this function yields two clear, non-uniform changes around 355 and 445 K for the lattice parameters *a* and *c* and at least one for *b* around 450 K (Fig. 9).

## Discussion

### *Structural changes in Pb-lawsonite*

The structural transitions of lawsonite with changing temperature, discovered initially by Libowitzky and Armbruster (1995), have been studied in great detail and found to be quite complex (Meyer *et al.*, 2001; Carpenter *et al.*, 2003; Sondergeld *et al.*, 2005; Carpenter, 2006; Salje and Carpenter, 2011; Salje *et al.*, 2011; Pavlov, 2013). Combining the results of an earlier study of phase transitions of hennomartinite (Sr-$Mn^{3+}$-lawsonite; Libowitzky and Armbruster, 1996) and the present paper, it becomes clear that incorporation of larger cations such as $Sr^{2+}$ and $Pb^{2+}$ in $Ca^{2+}$ sites leads to a shift of phase transitions to higher temperatures (lawsonite $T_C \approx 150$, 273 K; hennomartinite $T_C \approx 368$, 423 K; Pb-lawsonite $T_C \approx 355$, 445 K). However, with a different space-group evolution in the present case it is necessary to consider different structural transition behaviour. It is obvious that the phase transition of Pb-lawsonite around 445 K is related to a change of space group from *Pbnm* to *Cmcm*. To gain the relative and absolute atom displacements for every atom during the transitions the software *COMPSTRU* (Tasci *et al.*, 2012) was applied to the fractional atom coordinates of Tables 3, 5 and 6. At first this program searches for a transformation that best matches the lattice parameters of both structures to be compared. A structure transformation is achieved by determining the best pairing of the atom positions of the two structures using a suitable Euclidean normalizer. The results of this atom displacement analysis are plotted in Fig. 10.

A comparison of the structure at 370 and 488 K reveals a maximum displacement of the atom positions of O5w (≈ 0.40 Å) followed by O1 (≈ 0.2 Å), both in the **a** direction. Atoms O2 and O6,

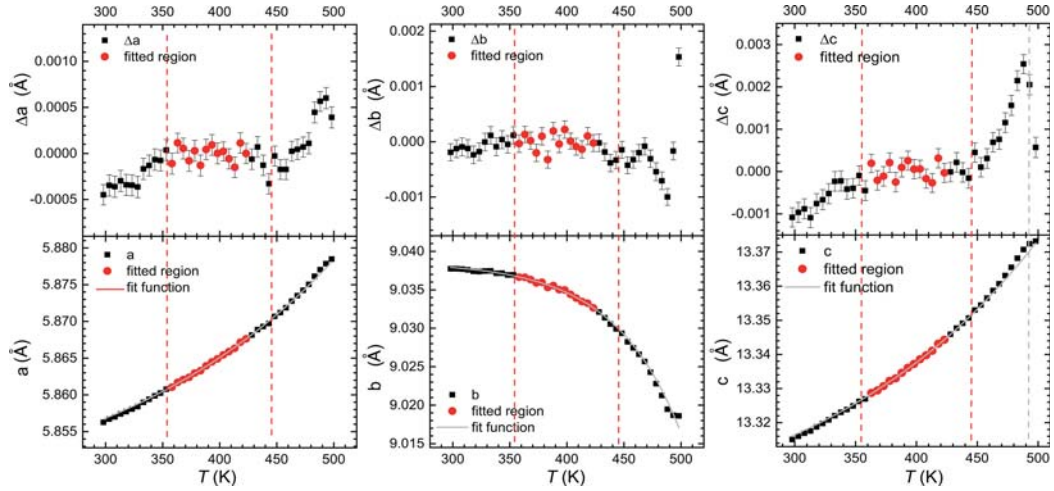


FIG. 9. Lattice parameters *a*, *b*, *c* versus temperature. The lower plots show the original parameters and an exponential decay function fitted to the central (marked) data points. The upper plots show the differences between the fit functions and the data points. The dashed lines mark the transition temperatures that were obtained from the principal component analysis plus subsequent cluster analysis of the diffraction patterns.

which are part of the $AlO_6$ octahedron and are merged into the same crystallographic position for the 488 K structure, show a total displacement ($u = u_x + u_y + u_z$) of ~0.12 and 0.13 Å, respectively. O4h of the hydroxyl group shows a u value of ~0.14 Å. However, hydrogen atom displacements cannot be determined by X-ray data alone. The mentioned shift of O1, the bridging atom in the silicate dimer, is accompanied by a small variation of the Si–O1–Si angle (154.90(5)° for 298 K; 155.31(20)° for 370 K; 154.02(21)° for 488 K). It should be noted that the Si–O1–Si angle of the 488 K structure refinement is biased by a high uncertainty caused by the use of powder XRD data. In the powder diffraction analysis the Si–O and O–O distances had to be restrained and refined with fixed isotropic displacement parameters. Nevertheless, the temperature-induced change of this angle is supported by an analysis of the band position of the Raman mode around 446 $cm^{-1}$ (RT) in Fig. 11. In their study of hemimorphite, which has similar $Si_2O_7$ dimers as lawsonite but no $AlO_6$ octahedra, Frost *et al.* (2007) assign a band at 451 $cm^{-1}$ to an Si–O–Si out-of-plane bending vibration. Consequently, the band at 446 $cm^{-1}$ (RT) in Pb-lawsonite could also result from

TABLE 6. Refined fractional atomic coordinates of orthorhombic Pb-lawsonite at 488 K (space-group setting *Cmcm*). The isotropic displacement parameters in the powder diffraction measurements are those of the 370 K refinement.

| Atom | Wyckoff | *x* | *y* | *z* |
|---|---|---|---|---|
| Pb | 4c | 0.5 | 0.16102(14) | 0.25 |
| Si | 8f | 0 | 0.01252(50) | 0.13094(31) |
| Al | 8d | 0.25 | 0.25 | 0 |
| O1 | 4c | 0 | 0.0282(15) | 0.75 |
| O2 | 16h | 0.2281(11) | 0.10712(65) | 0.10479(36) |
| O3 | 8f | 0 | –0.1463(12) | 0.07258(48) |
| O4h | 8f | 0 | 0.3476(13) | 0.05224(48) |
| O5w | 4c | 0 | 0.3759(15) | 0.25 |

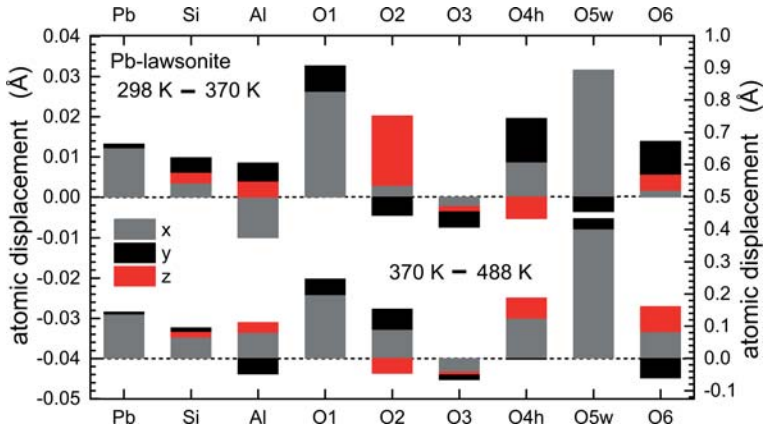


FIG. 10. Changes in positional parameters of Pb-lawsonite from room temperature (space group *Pbnm* – upper bars) to 370 K (*Pbnm*) to 488 K (*Cmcm* – lower bars).

bending/out-of-plane bending vibrations of Si–O–Si. Moreover, during the 445 K transition the 446 $cm^{-1}$ band shows nearly the same behaviour as the γ-OH vibration at ~858 $cm^{-1}$ (Figs 5 and 11), which is the most strongly shifted Raman band <1100 $cm^{-1}$. This implies that the Si–O–Si bending/out-of-plane bending vibration is considerably affected by the transition around 445 K and also by the phenomenon around 355 K (Fig. 11). These in turn are related to the change of the bridging Si–O–Si angle between the $SiO_4$ tetrahedra, accompanied by merging/separation of the O2/O6 atoms linking $SiO_4$ and $AlO_6$ polyhedra. The positive slope of the excess *c* lattice parameter versus temperature (after background subtraction) below 355 K and above 445 K (Fig. 9) seems to be a further consequence of the less straightened Si–O–Si angle and therefore has the same origin. So far, the structural transition of Pb-lawsonite around 445 K can be considered as a predominantly displacive phase transition of the rather rigid mixed polyhedral framework probably not

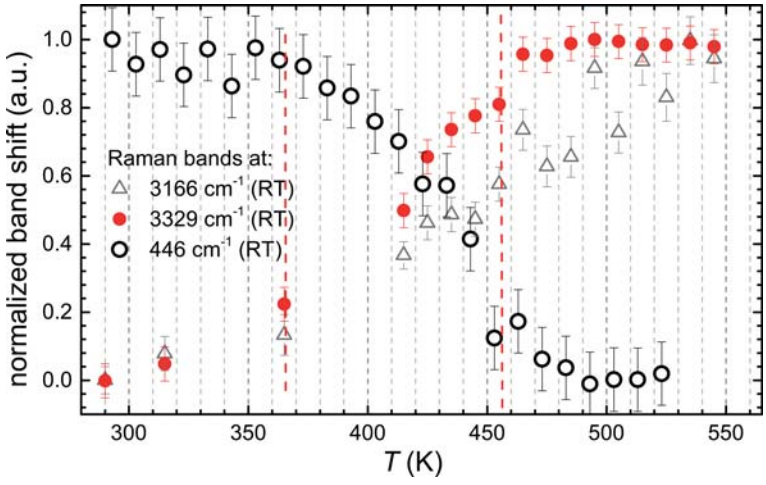


FIG. 11. Excess Raman band position of the δ/γ-Si–O–Si band at 446 $cm^{-1}$ (RT). The non-uniform change around 355 K is not obvious at first sight, but the 445 K transition is well defined. Also visible is the temperature-induced evolution of the Raman shift of the hydroxyl-group stretching vibration at 3329 $cm^{-1}$ (RT) *vs.* the band at 3166 $cm^{-1}$ (RT), probably belonging to a stretching vibration of the $H_2O$ molecule. Temperatures are slightly higher compared with the other Raman data, possibly caused by the use of a single crystal.

involving proton ordering/disordering processes. The latter can only be inferred from the strong non-uniform change of the $OH^-$ stretching band at 3329 $cm^{-1}$ (Fig. 5), caused by accompanying changes of H bonds. Structural changes around 355 K are generally weaker by an order of magnitude than those at the 445 K transition (Fig. 10). This is further supported by the small changes in the data curves in Figs 3, 4, 5, 7, 9, 10 and 11. The strongest atom displacement between 298 and 370 K is revealed by the O5w atom ($u_x >$ 0.03 Å) of the $H_2O$ molecule (Fig. 10). This is followed by the shifts of O1 ($u_x < 0.03$ Å), O2 ($u_z \approx 0.02$ Å) and O4h ($u_y$ and $u_x \approx 0.01$ Å) oxygen atoms. Thus, for the non-uniform changes around 355 K, the trend of atom displacement is roughly the same as for the 445 K transition, even if the magnitude is smaller.

### *Band assignments and suggestions from Raman spectroscopy*

In the Raman data, some similarities between lawsonite and Pb-lawsonite are observed. As the $H_2O$ molecule has a dipole moment and no centre of symmetry, all possible vibrations occur in Raman and IR spectra. If the data of Libowitzky and Rossman (1996) are compared with Figs 3 and 4 of the present work, it becomes obvious that Pb-lawsonite Raman spectra at RT are similar to lawsonite IR spectra at RT, presuming the high-energy bands of lawsonite around 3550 and 3612 $cm^{-1}$ are ignored. Moreover, in lawsonite an increase of temperature causes the bands at 3245 and 2960 $cm^{-1}$ (RT) to shift considerably to higher wavenumbers. Analogous behaviour is observed for the bands around 3329 $cm^{-1}$ and 3166/3210 $cm^{-1}$ (RT) in Pb-lawsonite. Table 7 compares O–O bond distances of the O4h, O2 and O5w oxygen atoms for the structure refinements of Pb-lawsonite at different temperatures. According to the correlation of stretching frequency and H-bond distances (Libowitzky, 1999) the change of the O4h···O2 hydrogen-bond distances from 2.73 Å (RT) to 2.92 Å (488 K) in Pb-lawsonite is expected to cause a theoretical band shift from ~3250 to 3500 $cm^{-1}$. Figure 3 shows the band at 3329 $cm^{-1}$ (RT) shifting to 3468 $cm^{-1}$ at 488 K. Therefore, we assign the Pb-lawsonite Raman band at 3329 $cm^{-1}$ (RT) to a hydroxyl stretching vibration. The change of the distances is within error for the non-uniform change around 355 K, but becomes obvious for the 445 K transition (Table 7). The O4h···O2 distance in Pb-lawsonite (2.73 Å at RT) is considerably shorter than the O4h···O4h distance (3.15 Å at RT) even at 488 K (2.92 Å *vs.* 3.08 Å) and it is slightly shorter than the O4h···O4h distance in lawsonite (2.75 Å). These distance constraints between potential donor and acceptor O atoms could be the reason for the different orientation of the hydrogen bonds of the OH groups in lawsonite versus Pb-lawsonite. The correlation between hydrogen-bond distances and wavenumbers of O–H stretching modes (Libowitzky, 1999) is used for the prediction of a stretching vibration of the $H_2O$ molecule as well. The bond distances at RT are 1.95(9) Å for d(Hw···O4h) [overestimated due to a too short O5–Hw distance] and 2.635(3) Å for d(O5w ···O4h) [underestimated due to the bent geometry of O5–Hw···O4h]; this suggests wavenumbers of ~3380 and 2950 $cm^{-1}$ and thus an averaged value of 3165 $cm^{-1}$. Figure 3 shows two bands at 3166 $cm^{-1}$ and 3210 $cm^{-1}$ (RT). The former seems to have different behaviour for the temperature evolution compared to the hydroxyl stretching vibration (3329 $cm^{-1}$; Fig. 11) and different behaviour in comparison to the γ-OH vibration at 858 $cm^{-1}$.

TABLE 7. Hydrogen-bond distances [Å] in Pb-lawsonite.

| | d(O4h···O2) | d(O4h···O4h) | d(O5w···O4h) |
|---|---|---|---|
| 298 K | 2.725(4) | 3.149(4) | 2.635(3) |
| 370 K | 2.733(13) | 3.139(13) | 2.633(11) |
| 488 K | 2.919(11) | 3.083(15) | 2.656(7) |

Compared to lawsonite, the *Cmcm* space-group symmetry of Pb-lawsonite should result in only one hydroxyl stretching band and two closely spaced (symmetric and antisymmetric) stretching bands of the $H_2O$ molecule. Thus, we consider the two bands at ~ 3200 $cm^{-1}$ to belong to the $H_2O$ stretching vibrations and the band at a higher wavenumbers to OH stretching. In Table 8, the assignments of the strongest O–H stretching vibrations for Pb-lawsonite are listed and compared to lawsonite. The *Cmcm* structure of lawsonite should result in a similar Raman/IR spectrum to that of high-temperature *Cmcm* Pb-lawsonite. However, as indicated by numerous previous investigations, the $H_2O$ and OH groups are dynamically disordered in lawsonite. The single H sites are close to those of the low-temperature *Pmcn* structure (Libowitzky and Rossman, 1996; Kozlova and Gabuda, 2013).

TABLE 8. Assignment of the strongest O–H stretching vibrations of Pb-lawsonite compared to lawsonite (Libowitzky and Rossman, 1996) at RT.

| Raman band position Pb-lawsonite ($cm^{-1}$) | Band assignment | IR band position lawsonite ($cm^{-1}$) |
|---|---|---|
| – | $\nu$-$H_2O$[a] | 3612 |
| – | $\nu$-OH[a] | 3550 |
| 3329 | $\nu$-OH | 3245 |
| 3210 | $\nu_3$-$H_2O$ | 2960 |
| 3166 | $\nu_1$-$H_2O$ | |

[a]caused by disordered hydrous species.

Thus it results in two high-energy stretching modes (no or weak H bonding) and two low-energy modes (strong H bonding) in the Raman spectra. As there is no high-energy Raman band in Pb-lawsonite, in either *Pbnm* or in *Cmcm*, this phase seems to lack disordered hydrous species with additional weak H bonds and therewith an oscillation of the $H_2O$ molecule between two equivalent sites. Distances between the $H_2O$ oxygen (O5w) and the H-bond acceptor (O4h) do not change remarkably during the phase transitions (2.636(3) – 2.633(11) – 2.656(7) Å, Table 7). There is no need for the $H_2O$ molecule and the OH groups to order/disorder as implied by the missing disordered hydrogen sub-lattice. It seems that the hydrogen atoms of the $H_2O$ molecules oppose the 445 K transition by enhancing hydrogen bonds, and this could cause the non-uniform changes in Raman band shifts around 355 K. Furthermore, the non-uniform change in Fig. 11 around 355 K is more distinct for the vibrational mode at 3166 $cm^{-1}$ ($\nu_1$ of $H_2O$) than for the 3329 $cm^{-1}$ band ($\nu$ of OH). Nevertheless, the phase transition in hennomartinite ($SrMn_2[(OH)_2|Si_2O_7]\cdot H_2O$), which is also of the lawsonite type and which has a similar rigid framework to lawsonite (Libowitzky and Armbruster, 1996), provides another potential explanation. In the low-temperature structure ($P2_1cn$) of hennomartinite, twinning parallel to (100) was found and it was assumed that the ordering of $H_2O$ and OH groups does not occur in the same way within the entire crystal, but rather ranges from local disorder to extensive twin domains (Libowitzky and Armbruster, 1996). This phenomenon could hold for Pb-lawsonite as well. In particular, the anisotropic displacement parameters of the RT structure of Pb-lawsonite, especially with respect to O5w ($U^{11} \approx 0.024(2)$, $U^{22} \approx 0.018(2) \rightarrow U_{eq} \approx 0.017(1)$ Å) compared with the value of the 370 K structure ($U_{iso} \approx 0.010(4)$ Å) supports this hypothesis. These stronger displacements at lower temperature could be a hint for such a domain development due to local disorder. However, instead of twinning a strong intergrowth of the Pb-lawsonite crystals was found in the single-crystal X-ray measurements at 298 and 370 K. This effect is caused by parallel growth of adjacent crystals, and no twinning was involved. In addition, the anisotropic displacement parameters of hennomartinite show different behaviour (Libowitzky and Armbruster, 1996).

### *Comparison of lawsonite and Pb-lawsonite transitions*

Libowitzky and Armbruster (1995) and Sondergeld *et al.* (2005) found that the coordinates of the framework atoms remain quite unchanged during the two temperature-induced phase transitions of lawsonite. Thus the transition of Pb-lawsonite around 445 K is different from that of lawsonite at 273 K due to an obvious contribution of framework distortions in Pb-lawsonite and the loss of a different mirror plane, i.e. in Pb-lawsonite the mirror plane '*m..*' is lost, in lawsonite at < 273 K it is the mirror plane '*..m*'. Consequently, the Wyckoff positions in Pb-lawsonite and lawsonite below the higher-temperature phase transition are quite different. In both phases, the oxygen atom O2 splits from 16*h* to two 8*d* positions (O2 + O6). For the 445 K transition of Pb-lawsonite there is no further split, whereas in lawsonite for the 273 K transition all the 8*f* positions split to two 4*c* positions. This applies to Si, Al, O4h, O3 as well as the hydrogen atoms of the hydroxyl group and $H_2O$ molecule. The different behaviour of Pb-lawsonite during the phase transition compared to lawsonite is probably due to a widening of the structure channel, which consists of $AlO_6$ octahedral chains and $Si_2O_7$ dimers. This channel hosts the $Pb^{2+}$ cation ($Ca^{2+}$ in lawsonite) and the $H_2O$ molecule. Comparing the *Cmcm* structures of lawsonite and Pb-lawsonite, the straighter Si–O–Si angle (154° *vs*. 137°, Fig. 12) in Pb-lawsonite provides more space for the cation. This results in 12-fold coordination of the Pb ion, because six more remote atoms (O3 and the next but one O1 and O5 atoms) are shifted towards the Pb ion and six closer O atoms drift away, compared to distances in lawsonite (Fig. 13). With regard to Shannon (1976) the $Pb^{2+}$ cation has a large 1.49 Å

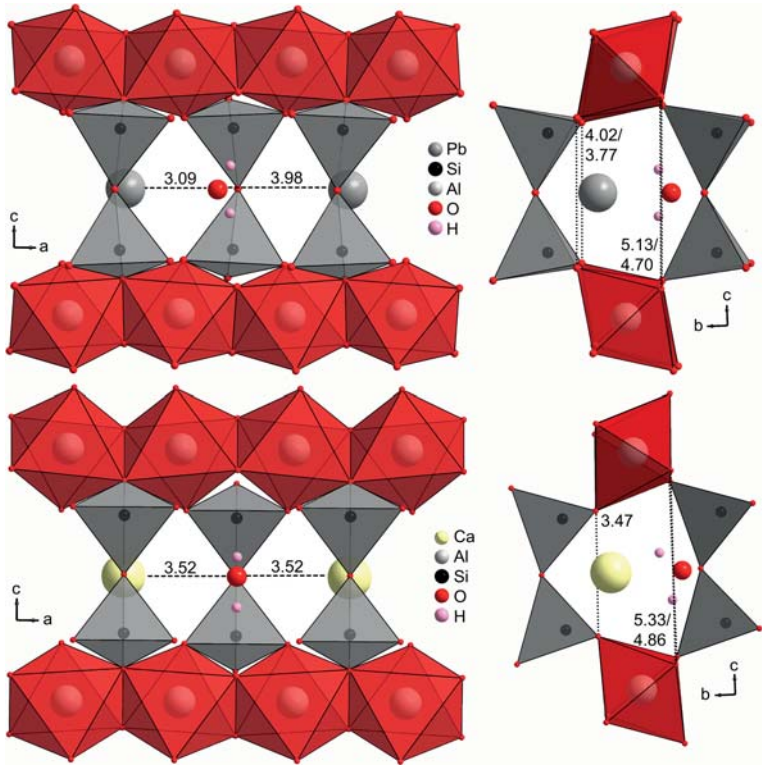


FIG. 12. Comparison of the structural channels of lawsonite (*Pmcn*, 233 K) and Pb-lawsonite (*Pbnm*, 298 K) hosting the Ca/Pb cation and the $H_2O$ molecule, in two different orientations. Numbers denote the interatomic distances in Å. Note the straightened Si–O–Si angle in Pb-lawsonite, resulting in a more circular cross-section of the channel.

theoretical effective ionic radius in ideal 12-fold coordination. This is much larger compared with an effective ionic radius of 1.00 Å for a $Ca^{2+}$ cation in ideal six-fold coordination. It could be that the O2 and Pb atoms come too close to each other below 445 K. Whatever the reason, the Pb atom is moved slightly out of its position and the O2 position is split into O2 + O6 (Fig. 13). As a consequence the '*m*..' mirror plane is lost, but the '..*m*' mirror plane, which is lost in lawsonite around 273 K, is preserved. In addition, the distance of 3.52 Å between Pb and the next nearest neighbour O5w drops to 3.09 Å, while the other O5w atom distance increases to 3.98 Å. Thus the $H_2O$ molecule is pulled out of the '*m*..' mirror plane as well. The same happens with the next-nearest neighbour O1 atoms, but the shift is not as pronounced as for the O5w distances (Fig. 13). These shifts result in an irregular ten-fold coordination of the $Pb^{2+}$ cation (Fig. 13). As a consequence, the theoretical effective ionic radius of the $Pb^{2+}$ cation falls to 1.40 Å. If the Pb–O1 bond of 3.42 Å is included in the Pb coordination (resulting in $Pb^{[11]}$) the theoretical effective ionic radius would fall to 1.45 Å. Dörsam *et al.* (2011) assumed a possible higher coordination of Pb compared to the six-fold coordination of Ca in the RT structure of lawsonite, but they only included the O3 atoms in the coordination sphere, and ignored the O5w and O1 atoms.

The abovementioned widening of the framework channel on one side (O2···O2, O6···O6) leads to a shrinkage on the other side (O3···O3, O4h···O4h; Fig. 12). This shrinkage is the reason for the different behaviour of the $H_2O$ molecule of Pb-lawsonite compared to lawsonite. Viewed along the *a* axis, the $H_2O$ molecule is located opposite the cation, though at a different 'height', in the framework channel (Fig. 12). On this side, the channel is shrunk, i.e. Pb-lawsonite has shorter distances between O3···O3 (4.70 Å) and O4h···O4h (5.13 Å) than those in lawsonite

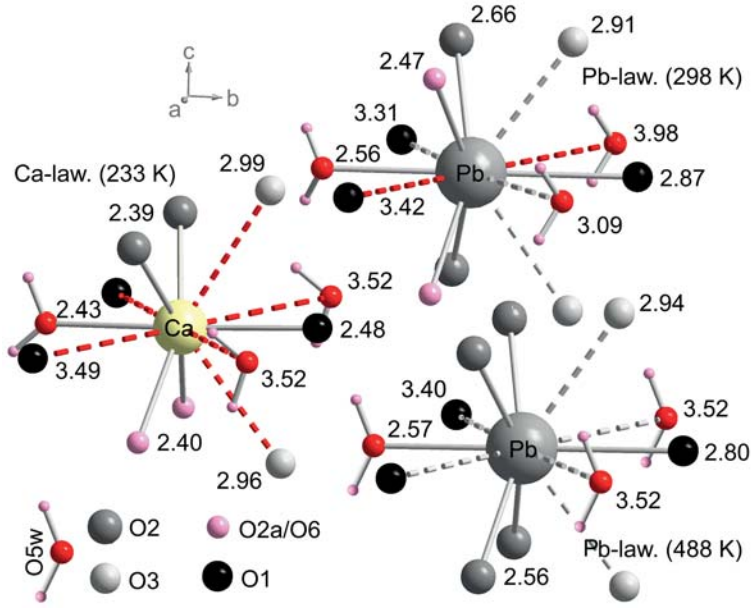


FIG. 13. Coordination around Ca and Pb in lawsonite and Pb-lawsonite. Dashed lines in grey show possible coordination bonds, while dashed lines in red show probably broken or absent bonds. Numbers denote bond lengths in Å.

(4.86 and 5.33 Å; Fig. 12). In lawsonite below 273 K the $H_2O$ molecule cannot be stabilized in the centre between the attractive forces of the remote H-bond acceptors O4h and O4ha. Thus it makes one short (Hw···O4h: 1.79 Å, Hw–O5w: 0.87 Å; respectively Hw···O4h: 1.70 Å with restrained Hw–O5w: 0.98 Å) and one long hydrogen bond (Hwa···O4ha: 2.27 Å, Hwa–O5w: 0.78 Å; respectively Hwa···O4ha: 2.22 Å with restrained Hwa–O5w: 0.98 Å), which breaks the '*..m*' mirror plane (Libowitzky and Armbruster, 1995; Libowitzky and Rossman, 1996). At room temperature, the $H_2O$ molecule in lawsonite oscillates between two equivalent sites similar to the ordered H positions below the phase transition at 273 K. The refined distance between Hwa···O4h is then 1.99 Å (Hwa–O5w: 0.80 Å) and with a restrained Hw–O5w distance of 0.98 Å it is 1.90 Å.

Due to comparably shortened Hw···O5w distances, the unrestrained values of lawsonite from Libowitzky and Armbruster (1995) can be better compared with the data of Pb-lawsonite refined here. The distance of Hw···O4h gained for Pb-lawsonite is 1.95 Å. The difference between 1.95 Å and 1.99 Å is not large, but in lawsonite, the value is distorted (to lower values) by the oscillation effect. Consequently, the apparent H–O–H angle of the $H_2O$ molecule in lawsonite at room temperature is 112.7° and thus unreasonably large. In Pb-lawsonite at room temperature, the angle of 105.9° almost matches the natural 104.5° angle of a free-water molecule (Császár *et al.*, 2005). Thus the average distance between Hw···O4h in the *Cmcm* structure of lawsonite is probably in the region of the average of the *Pmcn* structure of lawsonite (1.79 Å + 2.27 Å ≈ 2.03 Å), which is a minimum value as the $H_2O$ molecule has an angle of 107.6°. This small decrease of ≈0.1 Å from 2.03 Å in lawsonite to 1.95 Å in Pb-lawsonite has the effect that the $H_2O$ molecule can be stabilized in the centre between the two H-bond acceptors. Thus the $H_2O$ molecule does not seem to make one short and one long hydrogen bond resulting in the break of the '*..m*' mirror plane as in lawsonite (Fig. 12). Hydrogen bond behaviour could be also the reason for the phenomenon around 355 K, where the Raman shifts and lattice parameters versus temperature have a non-uniform change in slope. Indeed, below 445 K the O5w oxygen atom is pulled off the mirror plane '*m.*.'. Nevertheless, the Hw hydrogen atoms do not shift much due to slightly shortened hydrogen bonding with O4h (Table 7). Thus, the $H_2O$ molecule is rather tilted than shifted from the (100) plane at $x = 0$. This has no further effect slightly below 445 K, but with decreasing temperature and increasing shift of O5w accompanied by

increasing tilting of the $H_2O$ molecule, the enhanced hydrogen bonds begin to stop the atom shifts. This is supported by the strongest shifting Raman band, which probably arises from γ-OH vibrations (858 $cm^{-1}$ RT). It shows a similar strong wavenumber shift below and above 355 K, but in the region of 40 K around this temperature, it is relatively stable (Fig. 5, lower plot). The same constant behaviour applies for the Si–O–Si angle, the Raman shift of the δ/γ-Si–O–Si band and the *c* lattice parameter (Figs 9, 11). This temperature range with stabilized atom coordinates is probably caused by the hydrogen bonds, which are directed against the shift of O5w caused by its interaction with the $Pb^{2+}$ cation. It is concluded that the interaction of the large $Pb^{2+}$ cation with the tight framework of $AlO_6$ octahedra and $Si_2O_7$ dimers causes the structural transition around 445 K in Pb-lawsonite, where the coordination number of $Pb^{2+}$ is reduced from 12 to 10 or 11. A transition due to proton ordering/disordering as was found for the phase transitions of lawsonite (Libowitzky and Armbruster, 1995; Libowitzky and Rossman, 1996) is not suggested, even though the hydrogen bonds have a great impact on the behaviour of the phase transition in Pb-lawsonite.

## Acknowledgements

This work was supported by FWF grant P23108-N19. The authors are grateful for the opportunity to use the synchrotron single-crystal diffraction beam line of ANKA/KIT in Karlsruhe, Germany. Hans-Peter Nahbein (GFZ, Potsdam) is thanked for measuring X-ray diffraction powder patterns of very small samples. They appreciate the hints and comments given by referees Ross Angel and Günther Redhammer as well as the associate editor Mark Welch.

## References

Armbruster, T., Oberhänsli, R., Bermanec, V. and Dixon, R. (1993) Hennomartinite and kornite, two new $Mn^{3+}$ rich silicates from the Wessels Mine, Kalahari, South Africa. *Schweizerische Mineralogische und Petrographische Mitteilungen*, **73**, 349–355.

Brovarone, A.V. and Beyssac, O. (2014) Lawsonite metasomatism: a new route for water to the deep Earth. *Earth and Planetary Science Letters*, **393**, 275–284.

Carpenter, M.A. (2006) Elastic properties of minerals and the influence of phase transitions. *American Mineralogist*, **91**, 229–246.

Carpenter, M.A., Meyer, H.W., Sondergeld, P., Marion, S. and Knight, K.S. (2003) Spontaneous strain variations through the low temperature phase transitions of deuterated lawsonite. *American Mineralogist*, **88**, 534–546.

Cattell, R.B. (1966) The scree test for the number of factors. *Multivariate Behavioural Research*, **1**, 245–276.

Coelho, A.A. (2007) *TOPAS academic version 4.1.* Coelho software, Brisbane, Australia.

Császár, A.G., Czakó, G., Furtenbacher, T., Tennyson, J., Szalay, V., Shirin, S.V., Zobov, N.F. and Polyansky, O. L. (2005) On equilibrium structures of the water molecule. *Journal of Chemical Physics*, **122**, 214305.

Daniel, L., Fiquet, G., Gillet, P., Schmidt, M.W. and Hanfland, M. (1999) P-V-T equation of state of lawsonite. *Physics and Chemistry of Minerals*, **26**, 406–414.

Dörsam, G., Liebscher, A., Wunder, B., Franz, G. and Gottschalk, M. (2011) Synthesis of Pb-zoisite and Pb-lawsonite. *Neues Jahrbuch für Mineralogie – Abhandlungen*, **188**, 99–110.

Farmer, V.C. (1974) *The Infrared Spectra of Minerals.* Mineralogical Society, London.

Frost, R.L., Bouzaid, J.M. and Reddy, B.J. (2007) Vibrational spectroscopy of the sorosilicate mineral hemimorphite $Zn_4(OH)_2Si_2O_7{\cdot}H_2O$. *Polyhedron*, **26**, 2405–2412.

Gabelica-Robert, M. and Tarte, P. (1979) Synthesis, X-ray diffraction and vibrational study of silicates and germanates isostructural with kentrolite $Pb_2Mn_2Si_2O_9$. *Journal of Solid State Chemistry*, **27**, 179–190.

Hahn, T. (2005) *International Tables for Crystallography Volume A: Space-group Symmetry.* Corrected reprint of the fifth edition, Wiley, New York.

Hofmeister, A.M., Hoering, T.C. and Virgo, D. (1987) Vibrational spectroscopy of beryllium aluminosilicates: heat capacity calculations from band assignments. *Physics and Chemistry of Minerals*, **14**, 205–224.

Kawachi, Y. and Coombs, D.S. (1996) Noélbensonite, a new BaMn silicate of the lawsonite structure type, from Woods mine, New South Wales, Australia. *Mineralogical Magazine*, **60**, 369–374.

Kieffer, S.W. (1979) Thermodynamics and lattice vibrations of minerals: 3. Lattice dynamics and an approximation for minerals with application to simple substances and framework silicates. *Reviews of Geophysics and Space Physics*, **17**, 35–59.

Kieffer, S.W. (1980) Thermodynamics and lattice vibrations of minerals: 4. Application to chain and sheet silicates and orthosilicates. *Reviews of Geophysics and Space Physics*, **18**, 862–886.

Kozlova, S.G. and Gabuda, S.P. (2013) Single-crystal $^1H$ NMR data and hydrogen atom disorder in lawsonite, $CaAl_2[Si_2O_7](OH)_2{\cdot}H_2O$. *Journal of Structural Chemistry*, **54**, 146–151.

Larson, A.C. and Von Dreele, R.B. (1994) General Structure Analysis System (GSAS), *Los Alamos National Laboratory Report*, 86–748.

Lazarev, A.N. (1972) *Vibrational Spectra and Structure of Silicates.* Consultant Bureau, New York.

LeBail, A., Duroy, H. and Fourquest, J.L. (1988) Ab initio structure determination of $LiSbWO_6$ by X-ray powder diffraction. *Materials Research Bulletin*, **23**, 447–452.

Le Cléac'h, A. and Gillet, P. (1990) IR and Raman spectroscopic study of natural lawsonite. *European Journal of Mineralogy*, **2**, 43–53.

Libowitzky, E. (1999) Correlation of O-H stretching frequencies and O-H···O hydrogen bond lengths in minerals. *Monatshefte für Chemie*, **130**, 1047–1059.

Libowitzky, E. and Armbruster, T. (1995) Low-temperature phase transitions and the role of hydrogen bonds in lawsonite. *American Mineralogist*, **80**, 1277–1285.

Libowitzky, E. and Armbruster, T. (1996) Lawsonite-type phase transition in hennomartinite, $SrMn_2[Si_2O_7](OH)_2{\cdot}H_2O$. *American Mineralogist*, **81**, 9–18.

Libowitzky, E. and Rossman, G.R. (1996) FTIR spectroscopy of lawsonite between 82 and 325 K. *American Mineralogist*, **81**, 1080–1091.

Liebscher, A., Dörsam, G., Franz, G., Wunder, B. and Gottschalk, M. (2010) Crystal chemistry of synthetic lawsonite solid-solution series $CaAl_2[(OH)_2/Si_2O_7]{\cdot}H_2O$–$SrAl_2[(OH)_2/Si_2O_7]{\cdot}H_2O$ and the *Cmcm*-$P2_1/m$ phase transition. *American Mineralogist*, **95**, 724–735.

Mejía-Uriarte, E.V., Sato-Berru, R.Y., Navarrete, M., Kolokoltsev, O. and Saniger, J.M. (2012) Determination of phase transition by principal component analysis applied to Raman spectra of polycrystalline $BaTiO_3$ at low and high temperature. *Journal of Applied Research and Technology*, **10**, 57–62.

Mevel, C. and Kienast, J.R. (1980) Chromian jadeite, phengite, pumpellyite, and lawsonite in a high-pressure metamorphosed gabbro from the French Alps. *Mineralogical Magazine*, **43**, 979–984.

Meyer, H.W., Marion, S., Sondergeld, P., Carpenter, M.A., Knight, K.S., Redfern, S.A.T. and Dove, M.T. (2001) Displacive components of the low-temperature phase transitions in lawsonite. *American Mineralogist*, **86**, 566–577.

Miyajima, H., Matsubara, S., Miyawaki, R. and Ito, K. (1999) Itoigawaite, a new mineral, the Sr analogue of lawsonite, in jadeitite from the Itoigawa-Ohmi district, central Japan. *Mineralogical Magazine*, **63**, 909–916.

Novak, A. (1974) Hydrogen bonding in solids. Correlation of spectroscopic and crystallographic data. *Structure and Bonding (Berlin)*, **18**, 177–216.

Origlieri, M.J., Yang, H., Downs, R.T., Posner, E.S., Domanik, K.J. and Pinch, W.W. (2012) The crystal structure of bartelkeite, with a revised chemical formula, $PbFeGe^{VI}(Ge_2^{IV}O_7)(OH)_2{\cdot}H_2O$, isotypic with high-pressure $P2_1/m$ lawsonite. *American Mineralogist*, **97**, 1812–1815.

Pavlov, S.V. (2013) A phenomenological model of phase transitions in lawsonite. *Moscow University Physics Bulletin*, **68**, 139–142.

Pawley, A.R. and Allan, D.R. (2001) A high-pressure structural study of lawsonite using angle-dispersive powder-diffraction methods with synchrotron radiation. *Mineralogical Magazine*, **65**, 41–58.

Pearson, K. (1901) On lines and planes of closest fit to a system of points in space. *Philosophical Magazine*, **2**, 559–572.

Pechini, M.P. (1967) *Method of preparing lead and alkaline earth titanates and niobates and coating method using the same to form a capacitor.* US Patent 3,330,697.

Petříček, V., Dušek, M. and Palatinus, L. (2006) *JANA2006.* Institute of Physics, Prague.

Raab, S. (2010) *Synthese und Charakterisierung nanoskaliger hydraulisch hochreaktiver Phasen des Portland- und Tonerdezements.* PhD thesis, Martin-Luther-Universität Halle-Wittenberg, Germany.

Rietveld, H.M. (1967) Line profiles of neutron powder-diffraction peaks for structure refinement. *Acta Crystallographica*, **22**, 151–152.

Salje, E.K.H. and Carpenter, M.A. (2011) Thermally activated proton hopping in lawsonite, the ferroelectric transition at 125 K, and the co-elastic phase transition at 270 K. *Journal of Physics: Condensed Matter*, **23**, 112208.

Salje, E.K.H., Crossley, S., Kar-Narayan, S., Carpenter, M.A. and Mathur, N.D. (2011) Improper ferroelectricity in lawsonite $CaAl_2Si_2O_7(OH)_2{\cdot}H_2O$: hysteresis and hydrogen ordering. *Journal of Physics: Condensed Matter*, **23**, 222202.

Sato-Berru, R.Y., Mejía-Uriarte, E.V., Frausto-Reves, C., Villagrán-Muniz, M., Murrieta, S.H. and Saniger, J.M. (2007) Application of principal component analysis and Raman spectroscopy in the analysis of polycrystalline $BaTiO_3$ at high pressure. *Spectrochimica Acta*, **A66**, 557–560.

Schmidt, M.W. and Poli, S. (1994) The stability of lawsonite and zoisite at high pressures: experiments in CASH to 92 kbar and implications for the presence of hydrous phases in subducted lithosphere. *Earth and Planetary Science Letters*, **124**, 105–118.

Shannon, R.D. (1976) Revised effective ionic radii and systematic studies of interatomic distances in halides and chalcogenides. *Acta Crystallographica*, **A32**, 751–767.

Sheldrick, G.M. (2008) A short history of SHELX. *Acta Crystallographica*, **A64**, 112–122.

Sherlock, S.C. and Okay, A.I. (1999) Oscillatory zoned chrome lawsonite in the Tavşanlı Zone, northwest Turkey. *Mineralogical Magazine*, **63**, 687–692.

Sondergeld, P., Schranz, W., Tröster, A., Armbruster, T., Giester, G., Kityk, A. and Carpenter, M.A. (2005)

Ordering and elasticity associated with low-temperature phase transitions in lawsonite. *American Mineralogist*, **90**, 448–456.

Tasci, E.S., de la Flor, G., Orobengoa, D., Capillas, C. and Perez-Mato, J.M. (2012) An introduction to the tools hosted in the Bilbao Crystallographic Server. *EPJ Web of Conferences*, **22**, 1–22.

Toby, B.H. (2001) EXPGUI, a graphical user interface for GSAS. *Journal of Applied Crystallography*, **34**, 210–213.

Wondraschek, H. and Müller, U. (2010) *International Tables for Crystallography Volume A1: Symmetry Relations Between Space Groups.* Second edition, Wiley, New York.